JASA ARTICLE

Opportunistic ship source level measurements in the Western Canadian Arctic[a)]

Najeem Shajahan,[1,2,b)] William D. Halliday,[1,2] Jackie Dawson,[3] Ivor Maksagak,[4] Kyle Weese,[4] Humfrey Melling,[5] Andrea Niemi,[6] Svein Vagle,[5] Bill Williams,[5] and Stephen J. Insley[1,7]

[1]*Wildlife Conservation Society Canada, 169 Titanium Way, Whitehorse, Yukon Territory, Y1A 0E9, Canada*

[2]*School of Earth and Ocean Sciences, University of Victoria, Victoria, British Columbia, V8P 3E6, Canada*

[3]*Department of Geography, Environment, and Geomatics, University of Ottawa, Ottawa, Ontario, K1S 5B6, Canada*

[4]*Ekaluktutiak Hunters and Trappers Organization, Cambridge Bay, Nunavut, X0B 0C0, Canada*

[5]*Institute of Ocean Sciences, Sidney, British Columbia, V8L 5T5, Canada*

[6]*Freshwater Institute, Fisheries and Oceans Canada, Winnipeg, Manitoba, R3T 2N6, Canada*

[7]*Department of Biology, University of Victoria, Victoria, British Columbia, V8P 3E6, Canada*

ABSTRACT:

Increased ship traffic due to climate change increases underwater noise in the Arctic. Therefore, accurate measurements of underwater radiated noise are necessary to map marine sound and quantify shipping's impact on the Arctic ecosystem. This paper presents a method to calculate opportunistic source levels (SLs) using passive acoustic data collected at six locations in the Western Canadian Arctic from 2018 to 2022. Based on Automatic Identification System data, acoustic data, and a hybrid sound propagation model, the SLs of individual ships were calculated within a 5 km radius of each measurement site. A total of 66 measurements were obtained from 11 unique vessels, with multiple measurements from the same vessel type contributing more SLs. For vessels with propeller cavitation, measured SLs correlated positively with vessel parameters, such as speed and length. SL and speed did not correlate well for vessels without propeller cavitation. The JOMOPANS-ECHO SL model produced good agreement with measured SL for certain ship types (container ships, a tanker, and a passenger vessel). However, significant differences between measurement and model are evident for certain polar-class ships that travel in the Arctic, indicating that more controlled SL measurements are needed. © *2024 Acoustical Society of America*.

https://doi.org/10.1121/10.0026361

(Received 18 October 2023; revised 23 May 2024; accepted 30 May 2024; published online 13 June 2024)

[Editor: Klaus Lucke] Pages: 3807–3821

I. INTRODUCTION

The noise generated by transiting ships contributes significantly to low-frequency ambient sound in the ocean (Wenz, 1962). The influence of ship-generated noise can extend beyond low frequencies (<0.5 kHz) and reach several kilohertz at close ranges (Arveson and Vendittis, 2000), which include both wideband and narrowband components. Many factors can affect the frequency characteristics of ship noise, such as the design of the ship, the machinery on board, and the operational settings. The noise generated by propeller cavitation is dominant at low frequencies (<0.5 kHz), while noise generated by both propeller cavitation and machinery (engine, pumps, and generators) are dominant at mid to high frequencies (1–10 kHz) (Ross, 1976). The rapid growth of commercial shipping coupled with global economic development has been causing a gradual rise in yearly noise levels (NLs) at low frequencies in the northeast Pacific Ocean since 1950 (Ross, 2005; McDonald *et al.*, 2006; Chapman and Price, 2011; Frisk, 2012). Some recent studies have found a flattening or a reduction in yearly NL despite the growth of the shipping industry (Miksis-Olds and Nichols, 2016; Harris *et al.*, 2019). The increase in anthropogenic noise, especially from shipping, is an area of concern in bioacoustics and marine ecology (Duarte *et al.*, 2021; Chen *et al.*, 2021). Due to its wideband nature, ship noise has the potential to cause masking, changes in behavior, and physiological stress to many species of aquatic animals (Merchant *et al.*, 2014).

Identifying the excess contribution of shipping noise above the natural background sound is necessary to assess the potential exposure of anthropogenic noise on marine life. As part of existing methods, acoustic models are used to map the spatial dependence of underwater noise from ships (Erbe *et al.*, 2012, 2021; Merchant *et al.*, 2014; Farcas *et al.*, 2020). Very recently, passive acoustic data have been used in conjunction with the distribution of ships to identify regions of high exposure (Putland *et al.*, 2022). Noise mapping provides simulations of noise fields under hypothetical scenarios, as well as the ability to study underwater noise over wide areas and long time scales. To generate ship noise

[a)]"This paper is part of a special issue on Verification and Validation of Source and Propagation Models for Underwater Sound."

[b)]Email: najeemtkm@gmail.com

 © 2024 Acoustical Society of America

maps, environmental parameters for propagation loss (PL) modeling, information on ship traffic, and source levels (SLs) of ship are primary requirements. To compute noise maps in a particular area, either measured or modeled SL of various ship types can be used. Existing SL models are based on a combination of ship parameters to represent the broadband noise (Ross and Alvarez, 1964; Urick, 1983; Breeding *et al.*, 1996; Wales and Heitmeyer, 2002; Wittekind, 2014; MacGillivray and de Jong, 2021; MacGillivray *et al.*, 2022).

Recently, several studies have been reported comparing the measured SLs with available SL models (McKenna *et al.*, 2012, 2013; Simard *et al.*, 2016; Jansen and de Jong, 2017; Karasalo *et al.*, 2017). SLs of same vessel class varied significantly (up to 30 dB) in these studies possibly due to differences in noise measurement conditions (Chion *et al.*, 2019). The standard measurement procedure for SLs in deep water is based on American National Standards Institute (ANSI) and International Organization for Standardization (ISO) standards (ANSI S12.64, 2009; ISO 17208-1:2016, 2016; ISO 17208-2:2019, 2019). The ANSI/ISO standards recommends repeated simultaneous recordings using multiple hydrophones under constant operating conditions (speed, distance, water column depth, and position of hydrophones). There is also an ongoing effort to develop a standard procedure for measuring underwater radiated noise (URN) and modeling PL in shallow water (Ainslie *et al.*, 2022; MacGillivray *et al.*, 2022, 2023). SL measurement based on these standards provides minimal uncertainty. However, these methods require the cooperation of vessels under controlled conditions, making them challenging and expensive (Vendittis and Arveson, 2022).

A promising alternative for measuring SLs is to use opportunistic data from passive acoustic monitoring (PAM) systems. The ANSI/ISO standards do not define a standard approach to opportunistic measurements. Earlier opportunistic approaches used PAM measurements for a period between a few week to months, adhering as closely to ANSI/ISO standards as possible (McKenna *et al.*, 2012, 2013; Simard *et al.*, 2016; Jansen and de Jong, 2017; Karasalo *et al.*, 2017). Technological advancements have led to extended deployment periods, long battery life, and large storage capacities for PAM systems (Miksis-Olds *et al.*, 2018; Howe *et al.*, 2019). As a result, PAM systems deployed for longer periods in challenging environments can be used for opportunistic SL measurements. Long-term passive acoustic data can, however, introduce uncertainty in measured SLs due to duty cycle limitations and clock drift associated with hydrophones, large measurement distances, and uncontrollable ship operating conditions. This paper presents a methodology for measuring SLs opportunistically to address the limitations of long-term PAM data. We used acoustic data recorded in the Western Canadian Arctic from 2018 to 2022 by Wildlife Conservation Society Canada, Fisheries and Oceans Canada, and the Ekaluktutiak Hunters and Trappers Organization to determine SLs.

The Arctic Ocean is covered with ice for the majority of the year (Meredith *et al.*, 2019). Consequently, ships move through the Canadian Arctic, except predominantly during the summer and fall months (July through October) (Pizzolato *et al.*, 2016). As a result, the soundscape of the Canadian Arctic includes very little anthropogenic sound during the periods of ice coverage (Insley *et al.*, 2017; Halliday *et al.*, 2020, 2021). In recent years, however, the ice cover in the Arctic has diminished due to climate change, resulting in more extensive ice-free waters and a longer ice-free season (Li *et al.*, 2021; Stephenson *et al.*, 2011). Therefore, there has been an increase in the number of ships operating in this region (Pizzolato *et al.*, 2016; Eguiluz *et al.*, 2016), leading to an increase in underwater noise (Halliday *et al.*, 2021).

In previous studies, noise mapping methods have been used to understand and assess the impact of increased ship traffic on marine mammals in the Arctic (Halliday *et al.*, 2017, 2021, 2022; Aulanier *et al.*, 2017; Pine *et al.*, 2018). Nevertheless, studies focusing on the measurement of ship noise are needed to improve our understanding of the exposure of underwater noise from shipping on the Arctic ecosystem. As most ships passing through the Arctic are polar class vessels, their design and construction are subject to special standards which may result in undocumented SL characteristics. In recent years, the JOMOPANS-ECHO (J-E) SL model has gained wide acceptance for predicting ship noise and has been validated with a large database of measurements (MacGillivray and de Jong, 2021). However, the J-E model underrepresents or lacks vessels of the Polar class. Thus, the results of present analysis can also be used to assess the usefulness of existing SL models for ships traveling in the Arctic. In this study, we quantify and compare the SLs of ships operating in the Arctic based on satellite Automatic Identification System (AIS) vessel positions, PL models, and acoustic data collected from PAM systems.

II. METHODS

A. Acoustic recordings

Passive acoustic measurements collected at six locations in the Canadian Arctic between 2018 and 2022 were used for the analysis. The locations of passive acoustic recording sites are shown in Fig. 1, and metadata for the recordings are presented in Table I. At these locations, passive acoustic data are typically collected for a full year, although one dataset collected in the Kitikmeot Region was only for 6 weeks in September to October 2021. In this study, SL calculations are based on data recorded during ice-free summer periods (typically August to October), which is the only time of year when vessels are present in this region. All acoustic recorders were fixed to bottom-mounted oceanographic moorings, with hydrophones positioned 1–5 m above the seabed. Acoustic recorders had different duty cycles, ranging from ∼5 min per hour to continuous, but the most common duty cycle was 5 min every half hour (Table I). All hydrophones showed flat sensitivity

https://doi.org/10.1121/10.0026361

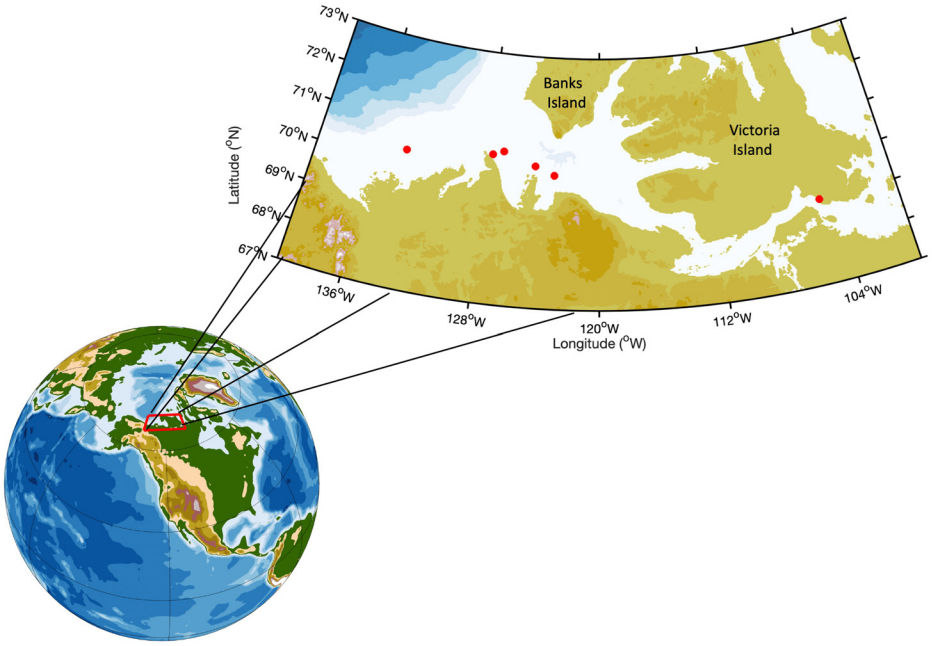

FIG. 1. (Color online) Locations of passive acoustic measurements (red dots) within the Western Canadian Arctic.

in the frequency range of 20 Hz to 10 kHz. Recorder types include Ocean Instruments SoundTrap ST500 and ST600 (Ocean Instruments NZ, Auckland, New Zealand).

B. AIS information

The characteristics of ship movements near a measurement location were derived from satellite AIS data (Spire Global, Inc., Ontario, Canada). For each ship, AIS data include a time stamp, speed, heading, GPS coordinates, as well as a maritime mobile service identity number and ship name. For SL estimation, AIS information within a 5 km radius of the measurement location was considered. In order to produce a time-dependent closest point of approach (CPA), the extracted AIS data were interpolated every second. This AIS position information was used to determine the radial distance between the ship and the hydrophone at times when the recorder was recording (i.e., accounting for the duty cycle) for PL calculations.

C. PL modeling

URN (radiated NL and SL) from ships, especially the radiated NL at a specific distance in deep water, can be calculated from received sound pressure level (SPL) and PL based on inverse square law (20 $\log_{10}$ distance) (ANSI S12.64, 2009; ISO 17208-1:2016, 2016). Radiated NL measured in deep water can be converted to monopole SL by applying a corrected formulae considering the Lloyd's mirror effect (ISO 17208-2:2019, 2019). However, in an acoustically complex shallow water environment, this single-parameter(range) model may not be appropriate for calculating PL. Thus, it is necessary to consider the sound speed in the water column, the change in bathymetry, the properties of the seabed, and volume absorption for accurate calculation of PL. Both sophisticated numerical models and simplified correction formulas can be used to estimate PL of URN measurements in shallow water (Ainslie *et al.*, 2022; MacGillivray *et al.*, 2023).

TABLE I. Deployment details of passive acoustic data collection from the Western Canadian Arctic between 2018 and 2022. Duty cycle is listed as time recorder is on and total time for the cycle to repeat (i.e., to calculate time off, subtract time on from total time).

Location	Latitude (°N)	Longitude (°W)	Deployed	Retrieved	Water column depth (m)	Sensor depth (m)	Recorder type	Sample rate (kHz)	Duty cycle
Mackenzie Shelf	70.3339	−133.74	2021-09-13	2022-10-05	55	53	ST600	48	5 min/30 min
Kitikmeot	69.038	−105.197	2021-09-01	2021-10-12	30	29	ST600	48	5 min/5 min
Cape Bathurst (50)	70.5757	−127.661	2018-10-07	2019-09-27	49	43.5	ST500	48	5 min/60 min
Cape Bathurst (50)	70.5766	−127.661	2019-09-27	2020-09-19	48	45	ST500	48	5 min/60 min
Cape Bathurst (50)	70.57957	−127.637	2021-09-12	2022-10-04	62	58	ST600	48	5 min/30 min
Cape Bathurst (300)	70.681	−126.872	2018-09-30	2019-09-27	295	289.5	ST500	48	5 min/60 min
Cape Bathurst (300)	70.681	−126.872	2019-09-28	2020-09-20	293	290	ST500	48	5 min/60 min
Cape Bathurst (300)	70.68115	−126.871	2021-09-12	2022-10-05	292	288	ST600	48	5 min/30 min
Pearce Point	70.2	−123.158	2018-10-02	2019-09-28	351	348	ST500	48	5 min/60 min
Cape Parry	70.39363	−124.541	2021-09-10	2022-10-03	156	152	ST600	48	5 min/30 min

The depth of the water column at the acoustic measurement locations used in this study ranged from 30 to 350 m, and the frequency of interest was between 31.5 Hz and 10 kHz. The high-frequency approximation makes ray-based models ineffective for predicting PL at low frequencies (Jensen *et al.*, 2011). The use of a parabolic equation (PE) model at high frequencies is not feasible due to its high computational cost (Tappert, 1974; Jensen *et al.*, 2011). Therefore, this study uses a hybrid modeling approach to determine PL. For the each decidecade band, frequencies from 31.5 Hz to 10 kHz, the proposed modeling approach uses a PE model at frequencies below 1 kHz and a ray theory model at frequencies above 1 kHz. A range-dependent PE model based on the split-step Fourier algorithm using the wide-angle PE approximation was used at low frequencies and ray tracing model BELLHOP was used at high frequencies (Lin *et al.*, 2013; Porter *et al.*, 1987; Porter, 2016). In each decidecade band, PL was calculated for ten logarithmically spaced frequency lines and the band average was used.

Seabed was considered to be a fluid half-space, and a flat sea surface with no surface loss was considered. The mooring locations are mostly ice-free when vessels are present for this study, so we did not consider any effects of sea ice at the surface. The input parameters for the model are water-column sound speed profile, horizontally varying bathymetry, and the acoustic properties of the seabed. In order to represent the seabed, geoacoustic parameters, including compressional sound speed, density, and bottom loss, were required. The sediment composition for each measurement location was obtained from a recent study on sedimentary processes in the Canadian Arctic Archipelago (Lataief *et al.*, 2021), and the corresponding acoustic properties were derived from Hamilton's geoacoustic model (Hamilton, 1980; Jensen *et al.*, 2011). The bathymetry was derived from the Global Multi-Resolution Topography database (Ryan *et al.*, 2009). For the sound speed profile, conductivity, temperature, and depth (CTD) profiles obtained during mooring deployment were used.

D. Data processing

Typically, the spectral density level (SDL), SPL for decidecade bands, and broadband SPL are used as metrics for passive acoustic data processing. The acoustic terminology used in this paper followed ISO 18405:2017 (2017). As part of this study, the following methodology was used to calculate the monopole SL of ships transiting the Western Canadian Arctic:

(1) The AIS data were used to extract information about each ship, including its type, speed, latitude/longitude, length, and timestamp, within a radius of interest (5 km), and ensured that no other ship was present within that radius at the same time.
(2) To extract received level (RL) metrics with the recordings of ship transit, interpolated AIS distance-time curves were synchronized with the acoustic recordings.
(3) Based on interpolated AIS distance-time curve and acoustic measurement, the CPA and data window period (DWP) of each ship passing were determined. The ANSI/ISO measurement standard defines DWP as the time it takes a ship to travel a track length of $\pm 30^{\circ}$ with respect to the CPA. ANSI/ISO standards for DWP were followed when the CPA was closer (<1 km). For larger CPAs, however, the entire recording period (5 min) was used. At certain locations, clock drift associated with long-term acoustic recordings also contributed to error in CPA values. Acoustic data can be used to determine clock drift by aligning the Lloyd's mirror pattern center with the AIS distance-time curve. The acoustic timestamp was corrected for clock drift after determining the drift at a specific time through linear interpolation. Each recording was divided into 1 s samples, and a Hanning window with no overlap was applied to each sample to calculate SDLs at 1 Hz resolution. Based on power averaging across all 1 s samples in the DWP, RL metrics (SDL, SPL, and broadband SPL) were calculated for each ship noise recording. The SDL was calculated as

$$L_{p,f} = 10\log_{10}\left(\frac{S(f)}{p_0^2/f_0}\right)\text{dB}, \tag{1}$$

where p_0 is the reference pressure $(1\ \mu Pa)$ and the reference value f_0 is 1 Hz. $S(f)$ is the mean square sound pressure in a specified frequency band of the recorded time series. The SPL was computed between low (f_{lo}) and high (f_{hi}) frequency limits of the decidecade band as

$$L_p = 10\log_{10}\int_{f_{lo}}^{f_{hi}}\frac{S(f)}{p_0^2}\,df\ \text{dB}. \tag{2}$$

Broadband SPL was estimated by summing over all decidecade frequency bands (31.5 Hz to 10 kHz) as

$$L_{p,b} = 10\log_{10}\sum 10^{L_p/10}\,\text{dB}. \tag{3}$$

(4) Background NL adjustments were applied to the RL metrics using a set of criteria based on signal-to-noise ratio. The signal-plus-noise-to-NL difference (ΔL) was calculated for each decidecade band from 50 Hz to 1 kHz. If ΔL was less than 3 dB for more than three decidecade bands, the data were removed from further analysis; and if ΔL was greater than 3 dB for enough decidecade bands, the background sound level was subtracted to obtain the background noise-adjusted SPL (MacGillivray *et al.*, 2019):

$$L'_p = 10\log_{10}\left[10^{L_{p,s+n}/10} - 10^{L_{p,n}/10}\right]\text{dB}, \tag{4}$$

where $L_{p,s+n}$ is the total received SPL, $L_{p,n}$ is the background ambient SPL, and L'_p is the background noise-adjusted SPL of the ship. To calculate background ambient sound levels, either measured sound from the location with no ships in the area or an empirical

https://doi.org/10.1121/10.0026361

wind-generated noise model can be used. We used a site-dependent background noise model that depends on windspeed and frequency, and the details are given in Sec. III C.

(5) A PL map for each location on a fixed spatial grid was generated at the center frequencies of each decidecade bands from 31.5 Hz to 10 kHz. A frequency averaging was applied for 10 logarithmically spaced frequency lines (n) within each decidecade band, and the band average was used:

$$N_{PL,f} = 10\log_{10}\left[\frac{1}{n}\sum_{i=1}^{n} 10^{N_{PL}(f_i)/10}\right] \text{dB}. \quad (5)$$

(6) To determine PL between transiting vessels and the location of the acoustic recordings (N_{PL}), linear interpolation was applied to the PL map.

(7) In the final step, the L'_p and N_{PL} were combined to produce the monopole SL of a ship in decidecade bands:

$$L_s(f) = L'_p(f) + N_{PL}(f, r). \quad (6)$$

The measured ship source SDL can be calculated from SL in decidecade bands by subtracting the bandwidth:

$$L_{s,f}(f) = L_s(f) - 10\log_{10}\left(0.231 \times \frac{f}{1\,\text{Hz}}\right) \text{dB}. \quad (7)$$

III. RESULTS AND DISCUSSIONS

A. Vessel characteristics

The SL estimation criteria given in Sec. II D were met by 66 ship measurements from 11 unique ships. Among the 11 unique ships, seven ship types (classifications) were identified. Figures 2(a) and 2(b) show the number of measurements and unique ships for different ship types. Tug vessels, a fishing vessel, and a research vessel made up the majority of the measurements. However, multiple measurements of the same ship were included in the dataset, especially for a fishing and research vessel, and the highest number of unique ships for individual classes were from container ships and tugs. Figures 2(c)–2(e) illustrate the statistics about length, speed, and CPA distance for all the ship measurements. A mean length of 104 m was found in the data, with ships ranging from 39 to 173 m in length. Transit speed varied between ship classes, where a tanker traveled relatively fast with a median speed of 13 knots, whereas a research vessel traveled at a median of 3 knots. The distance between vessels and the hydrophone for SL estimates varied between 115 m and 5 km (the cut-off distance for our sample), with most measurements between 1 and 4 km.

B. PL calculation

We used an Nx2D approach that calculates PL as a function of range, azimuth, and depth without including azimuthal coupling (horizontal sound refraction). The hybrid

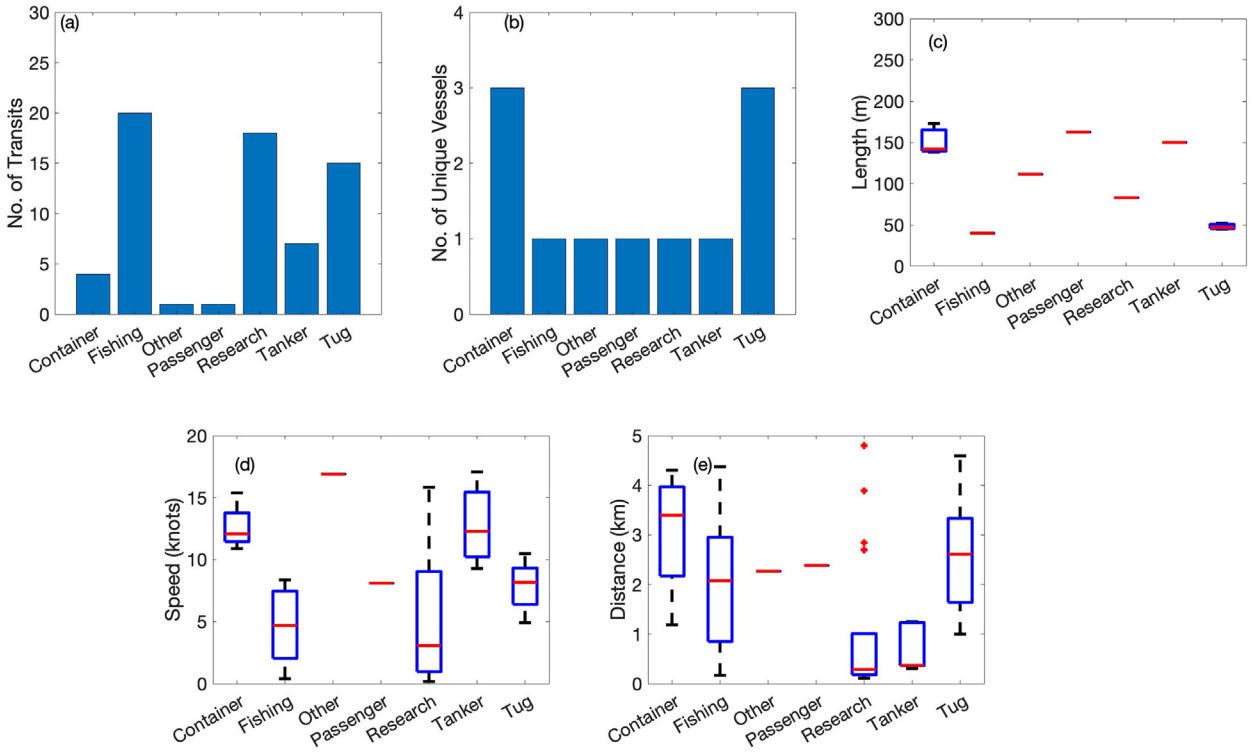

FIG. 2. (Color online) Statistics of vessel parameters used in the analysis. (a) Number of measurements. (b) Number of unique ships, box-whisker plots of nine ship types for (c) length, (d) speed over ground, and (e) distance to CPA. Red line inside the box shows the median. Ends of the box indicate the upper and lower quartiles. Black bar indicates the highest and lowest observations.

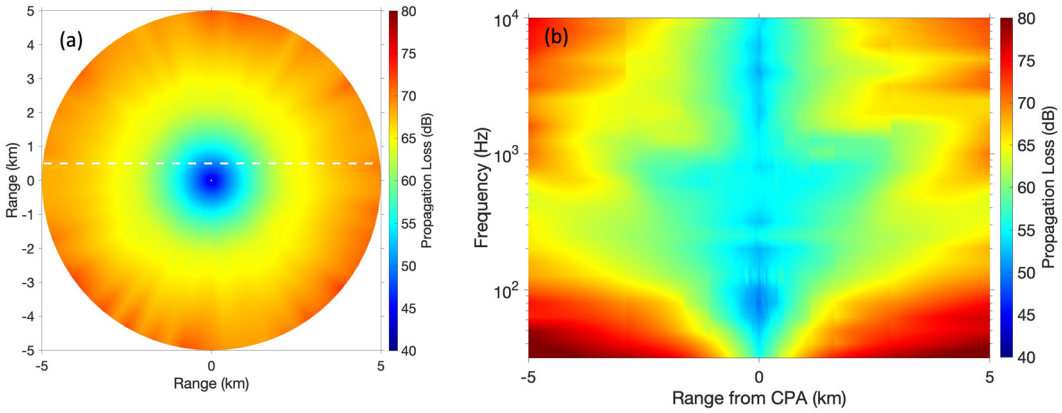

FIG. 3. (Color online) PL map for Cape Bathurst at (a)100 Hz and a hypothetical vessel track (white dashed line), and (b) the corresponding PL as a function of range and frequency for the selected track.

model described in Sec. II C calculates PL from a point source within a given radius (5 km) as a function of range for every 5° in azimuth. For the calculation of the PL map, the principle of reciprocity was invoked. In reciprocity, the pressure field remains the same regardless of the direction of propagation between two points, so the positions of sources and receivers can be changed (Jensen *et al*, 2011). By keeping a sound source at the hydrophone's depth, the pressure field as a function of range and azimuth at a point below the sea surface was determined (ship's source depth). To calculate PL between a ship's position and a hydrophone at specific frequencies, the positions of the receiver and source were swapped. We took 6 m for the ship's source depth, which is the average value of drafts reported in previous studies (Wales and Heitmeyer, 2002; Gassmann *et al*, 2017; Jansen and de Jong, 2017; MacGillivray and de Jong, 2021). To eliminate deep nulls in PL and effectively represent each decidecade band, a range averaging technique was also applied (Harrison and Harrison, 1995). The range averaged PL map at Cape Bathurst (300 m) station for 100 Hz is shown in Fig. 3(a). To extract PL as a function of range and frequency, a hypothetical ship track passing through the CPA at 500 m (white dashed line) was selected. The PL as a function of range and frequency for the selected track is shown in Fig. 3(b). Both sides of the CPA show gradual increase in PL with respect to the horizontal range.

A number of factors influence PL modeling, including bottom loss, sound speed profile, bathymetry, and source depth. Due to the lack of subsurface information at our measurement sites, we treated the seabed as a half-space with

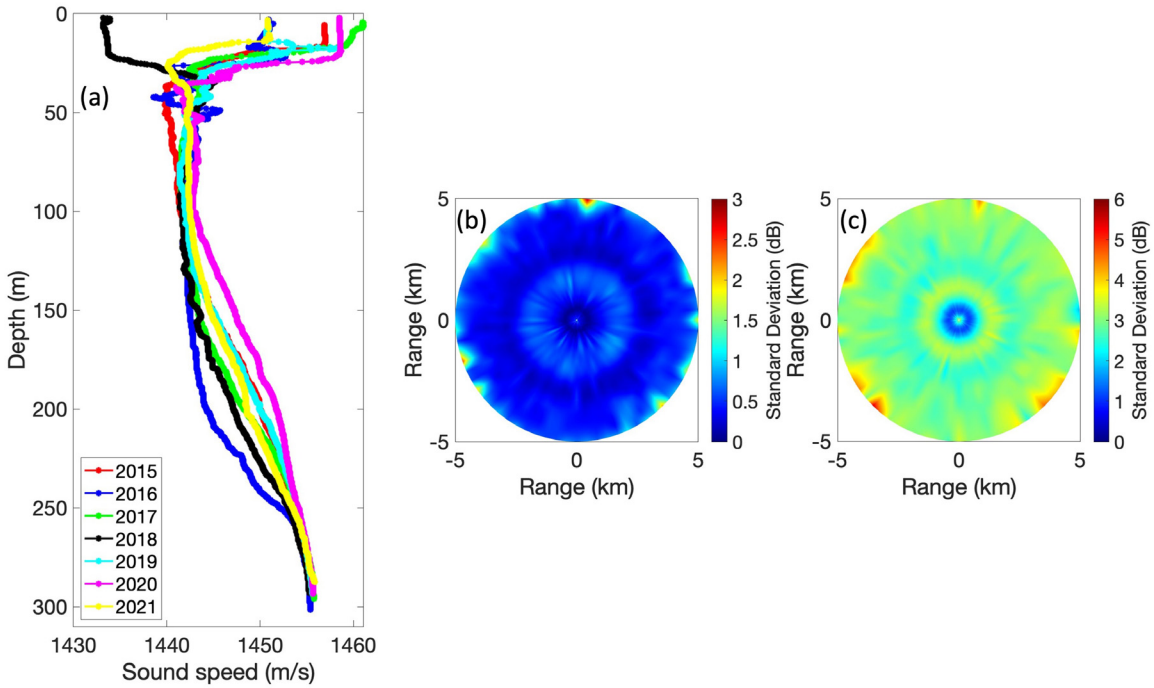

FIG. 4. (a) (Color online) Measured sound speed profiles near Cape Bathurst. (b) Corresponding standard deviations in PL maps at 100 Hz. (c) Standard deviations in PL maps at 100 Hz for sources ranging from 3 to 15 m deep.

https://doi.org/10.1121/10.0026361

uniform geoacoustic properties (compressional sound speed, density, and bottom loss). Acoustic properties of subsurface layers affect PL calculations at low frequencies. Another source of uncertainty in PL modeling is the time-varying sound speed profile during summer in the Arctic. PL modeling in this study was based on sound speed profiles measured close to measurement locations. SSP data collected from 2015 to 2021 near Cape Bathurst (300 m) were used to quantify the uncertainty in PL due to the sound speed profiles, as shown in Fig. 4(a). The standard deviation of the PL map at 100 Hz for Cape Bathurst is shown in Fig. 4(b). Variations in sound speed profiles have a relatively small impact on PL. There is a minimum deviation of 1 dB within 4 km and a maximum deviation of 2.5 dB beyond that. Changes in source depth can also have significant influence on PL calculations. Depending on the type and size of vessel, the depth of the ship noise source may range from 3 to 15 m (Gassmann *et al*, 2017). As a result, we calculated the standard deviation in the PL map by varying the source depth from 3 to 15 m, and the result is shown in Fig. 4(c). In short ranges (<0.5 km), the standard deviation is less than 1 dB; but beyond that range, it increases to an average of 4 dB.

The same approach was used to calculate PL of other noise measurement sites based on respective environmental data. When using long-term passive acoustic data collected near heavily trafficked shipping routes, PL maps are computationally advantageous for SL estimation. Once the position/track of the ship is known, precalculated PL map can be used as a lookup table instead of running the propagation model several times. Moreover, to account for the horizontal refraction of sound on SL estimates, the Nx2D approach can be replaced by a 3-D propagation model.

C. RL calculation

Using passive acoustic data from each measurement location, 5-minute averaged SDLs were derived for ship and wind noise analysis. AIS timestamps were used to separate data containing recordings of ship noise. Figure 5(a) shows the long-term spectrogram of Cape Bathurst (300 m) during the ice-free season of 2018. The RLs of ship noise were

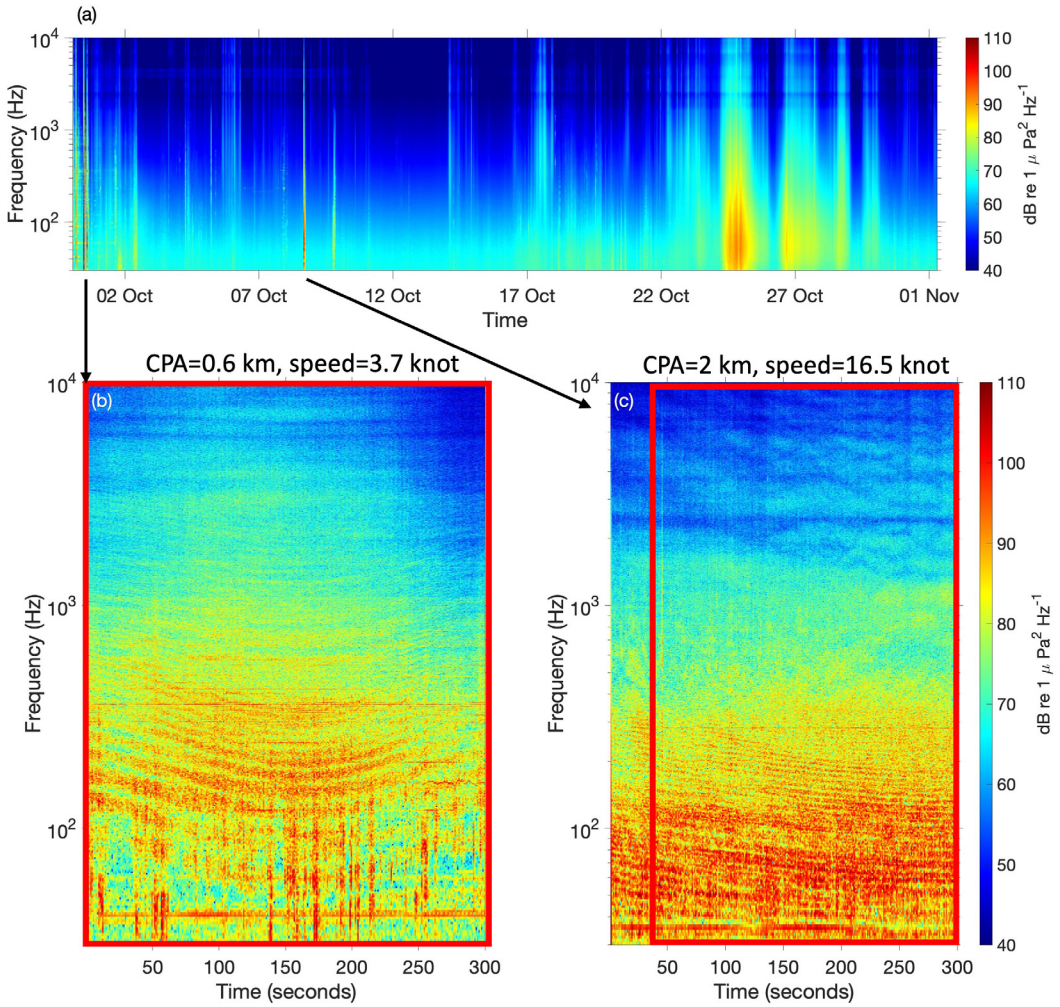

FIG. 5. (Color online) (a) Long-term spectrogram of passive acoustic data collected from Cape Bathurst (300 m) in 2018. (b), (c) Spectrogram of two ship passes and the corresponding DWP (red square).

calculated using data processing methodology (Sec. II D). Figures 5(b) and 5(c) show spectrograms of ship-generated noise at two separate occasions. The Canadian Arctic is dominated by wind-induced ambient sound in the summer, apart from occasional ship-generated noise (Insley *et al.*, 2017; Halliday *et al.*, 2020). The RLs of ship recordings can therefore be influenced by background noise. Thus, we developed a site-dependent background sound model as a function of wind speed and frequency based on hourly measurements of wind speed and NL. Wind speed data were obtained from European Centre for Medium-Range Weather Forecasts Reanalysis 5 reanalysis data close to the measurement locations every hour (Hersbach *et al.*, 2020). Previous empirical models of wind-generated noise established a clear functional relationship between windspeed (u) and NL (Ma *et al.*, 2005; Hildebrand *et al.*, 2021). We carried out linear regression as a function of frequency with both u and $\log_{10}(u)$ as independent variables.

Figure 6(a) shows the coefficient of determination (r^2) as a function of frequency between these two approaches for Cape Bathurst (300 m). There was a gradual increase in r^2 values up to 1 kHz, and then a constant value with moderate correlation followed. Almost similar values of r^2 were obtained from both approaches. We assumed a logarithmic relationship between wind speed and NL $(NL = C + 20 * n \log_{10}(u)$, where C is the y-intercept and n is the slope) at each location from 31.5 Hz to 10 kHz. Figure 6(b) shows the predicted NL at decidecade central frequencies at 7 m/s wind speed for the measurement locations. The background sound spectra for deep water locations (Cape Bathurst 300 m and Pearce Point) showed a gradual decrease in sound level with frequency, consistent with previously reported studies (Wenz, 1962; Vagle *et al.*, 1990). There was an increase in sound levels in the mid-frequency range in Kitikmeot. Surf sounds and proximity to the coast could be responsible for the increase in mid-frequency levels (Deane, 1997). Table II presents the slope, y-intercept, and r^2 values of the empirical model at selected decidecade central frequencies for all the measurement locations. Based on the signal-to-noise ratio criteria, the empirical models were used to remove background noise from RL using the measured wind speed at the time of ship passage.

D. SL calculation

The SLs for individual vessels at each decidecade band and the ship source SDLs for each measurement location were calculated from measured SPL and estimated PL using Eqs. (6) and (7). The URN of a ship can be attributed to machinery noise, flow noise, and propeller noise, which includes cavitation. At low speeds, machinery noise dominates, while cavitation dominates at higher speeds. The lowest cavitation inception speed in commercial vessels can be 8 knots (Leaper *et al.*, 2014). Using 8 knots as a threshold, we classified the measured SLs into non-cavitating and cavitating vessels.

1. Non-cavitating vessels

We obtained 37 measurements of SLs that are non-cavitating from three different types of vessels: a fishing vessel, a research vessel, and three tugs. The fishing vessel (17) contributed the most SL measurements, followed by a research vessel (13) and tugs (7). In Fig. 7(a), mean measured SL is shown for non-cavitating vessels as a function of frequency for different vessel types. Among all vessels,

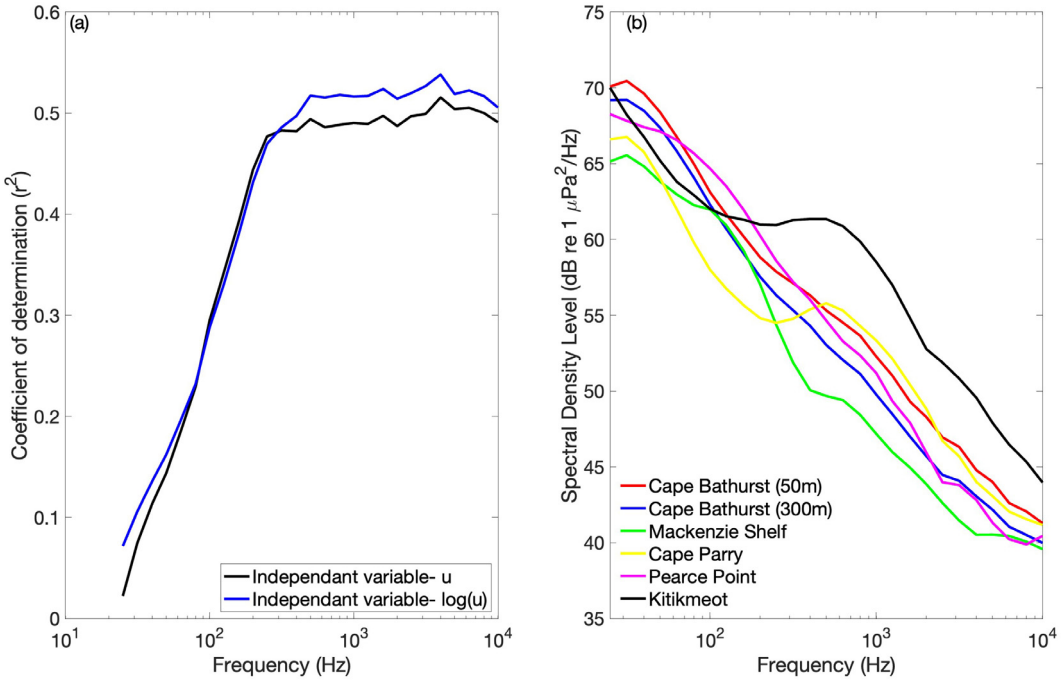

FIG. 6. (Color online) (a) Coefficient of determination as a function of frequency for Cape Bathurst. (b) Estimated wind NL in the decidecade frequency bands at an arbitrary wind speed of 7 m/s.

https://doi.org/10.1121/10.0026361

TABLE II. The slope, y-intercept, and r^2 values of background sound model for selected decidecade central frequencies.

Location	50 Hz	100 Hz	200 Hz	500 Hz	1 kHz	2 kHz	5 kHz
Mackenzie Shelf	0.74,58.6, 0.39	0.84, 56, 0.41	1.07, 49.5, 0.58	1.42, 39.6, 0.69	1.5, 36.6, 0.7	1.46, 33.6, 0.7	1.17, 32.3, 0.7
Pearce Point	0.05, 66.8, 0.02	0.13, 63.7, 0.07	0.44, 57.1, 0.33	1, 47.6, 0.6	1.1, 43.2, 0.6	1.2, 37.4, 0.63	1, 33.9, 0.62
Cape Bathurst (50)	0.64, 63.9, 0.17	0.82, 57.3, 0.31	0.96, 52, 0.46	1.1, 47.7, 0.51	1, 45, 0.5	1.1, 40.6, 0.51	0.9, 37.4, 0.53
Cape Bathurst (300)	0.49, 63.9, 0.16	0.71, 57.3, 0.29	0.9, 51.1, 0.43	1.1, 45.3, 0.52	1.1 42.3, 0.52	1.1, 38.1, 0.51	0.9, 35.8, 0.52
Kitikmeot	0.72, 60.8, 0.11	0.62, 62.6, 0.06	0.58, 64.7, 0.05	0.62, 61.7, 0.07	0.65, 57, 0.3	1.15, 43.3, 0.44	1.19, 35.4, 0.46
Cape Parry	0.25, 62.2, 0.23	0.78, 52.5, 0.5	1.03, 47.5, 0.63	1.13, 47.8, 0.67	1.16, 45.1, 0.68	1.25, 40, 0.72	1.17, 34.8, 0.73

tugs had the highest mean SL, and fishing vessel had the lowest. When towing a barge, tugs are likely to cavitate even at low speeds (<8 knots). The mean SL of different vessel types varied by 20 dB at frequencies below 1 kHz. For all vessel types, the frequency roll-off of mean SL above 1 kHz was nearly similar (6 dB/octave). The non-cavitating SL measurement's dependence on ship characteristics was examined using broadband SL (summing all decidecade frequency bands from 31.5 Hz to 10 kHz). Broadband SL measurements for different vessel types are plotted as a function of speed in Fig. 7(b). The maximum broadband SL in this class was recorded by the research vessel traveling at 1.8 knots. Figure 7(b) does not show a clear functional relationship between broadband SL and speed of various ship types. There is generally a linear relationship that exists between SL and a ship's speed (u) and length (l) in the $\log_{10}(u, l)$ space. A very weak relationship ($slope = 0.24$ and $r^2 = 0.01$) was found between SLs measured in the 125 Hz decidecade band and vessel speed for non-cavitating vessels. For vessels without propeller cavitation, a weak speed dependence may result from the dominant contribution of machinery noise. However, the measured SLs correlated positively ($slope = 20.4$ and $r^2 = 0.2$) with vessel length for the non-cavitating vessels.

The majority of existing ship SL models represent the broadband component of propeller cavitation. Thus, it is not appropriate to compare non-cavitating SLs with available SL models. Most of the SL measurements for the research vessel were obtained during the deployment and recovery of acoustic recorders. At low speeds and short ranges, machinery on board could have contributed more to the measured SLs. Radiated noise from machinery depends on vessel size, engine, and generator mounts, but identifying machinery's contribution to overall noise is challenging (Smith and Rigby, 2022). As a result of the ship type differences and the limited number of measurements obtained here, fitting a frequency-dependent empirical model to predict the non-cavitating SL of shipping in the Arctic may not be feasible.

2. Cavitating vessels

In the case of cavitating vessels, 29 SL measurements were obtained from 10 different ships. The most SLs were

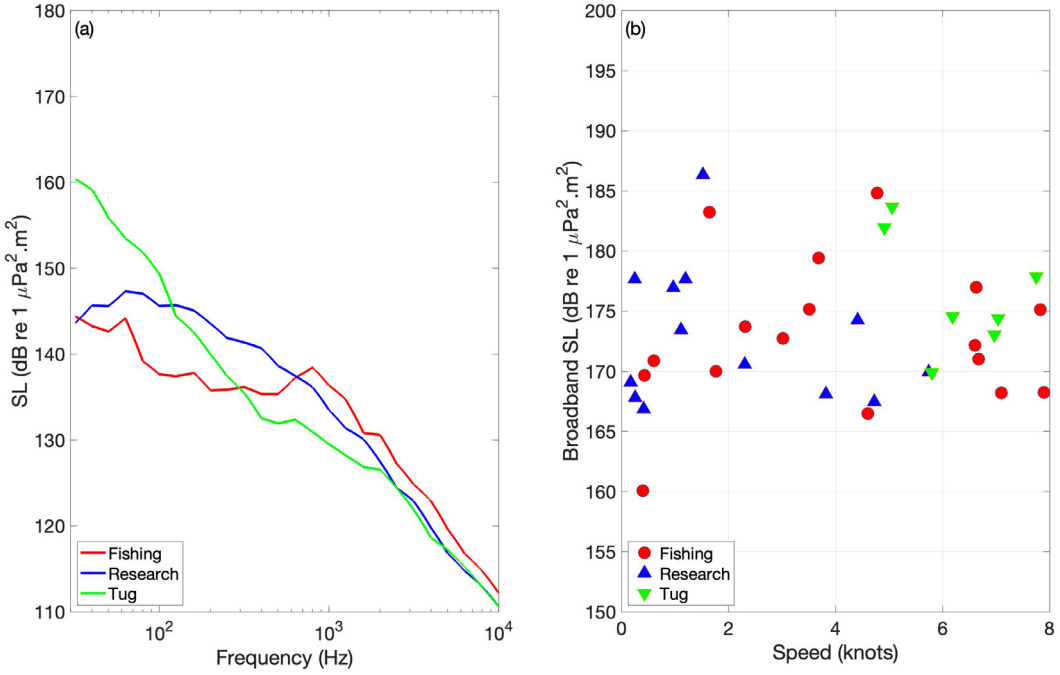

FIG. 7. (Color online) (a) The mean SLs of non-cavitating vessels for different vessel types. (b) The broadband SLs of non-cavitating vessels as a function of speed. Different symbols indicate the ship types.

contributed by two tugs (8) and a tanker (7). The other vessels contributing SLs were a research vessel (5), container ships (4), a fishing vessel (3), a passenger ship (1), and an icebreaker (1). SLs for different ship types for cavitating vessels are shown in Fig. 8(a). Fishing vessel exhibited the lowest value at frequencies below 100 Hz, while icebreaker exhibited the highest SL. Above 1 kHz, frequency roll-off followed a similar slope regardless of vessel type. Broadband SLs for cavitating vessels are shown in Fig. 8(b). Maximum broadband SL was recorded by a tanker traveling at 17 knots, and minimum broadband SL was recorded by a fishing vessel traveling at 8.5 knots. Cavitating vessels exhibit a gradual increase in SL with speed.

The available empirical SL models established a clear relationship between SL and ship properties, such as speed and length for cavitating vessels (MacGillivray *et al.*, 2019; MacGillivray and de Jong, 2021). A linear regression between SLs measured in the 125 Hz decidecade band and ship speed and length was conducted to determine the functional relationship between ship properties and SLs [Figs. 9(a) and 9(b)]. The slope of SL to speed in previous studies varied from 4 to 60 with a mean value of 48, and the slope of SL to length was 20 (Chion *et al.*, 2019). We also found a positive correlation $(r^2 = 0.17)$ between speed and SL with a slope value of $32\,(\pm 14)$ for all the cavitating SLs. Our slope estimate of SL to speed was comparable to those reported in recent studies (Chion *et al.*, 2019). In addition, the slope for SL to length also showed a positive correlation $(r^2 = 0.41)$ with a value of $22\,(\pm 5)$ that closely matches the results of existing models.

Measured SLs can be used to test the suitability of existing SL models in the Arctic. We investigated the applicability of two empirical SL models: J-E (MacGillivray and de Jong., 2021) and RANDI (Research Ambient Noise Directionality)-Breeding (R-B) (Breeding *et al.*, 1996), against measured SLs of cavitating vessels. A ship's individual SL can be expressed as a function of frequency, speed, and length with a reference spectrum based on the R-B model. With the J-E model, the baseline spectrum of R-B was modified to include the AIS ship type as a new input. We compared the measured SLs of individual vessels with the predictions from the J-E and R-B models. For each vessel, Fig. 10 shows the frequency averaged absolute residual difference between measured and predicted SLs. Measured SLs of a tanker, fishing vessel, research vessel, passenger ship, and container ships showed better agreement with J-E than R-B. For an icebreaker, the R-B model prediction matched measurement well compared to the J-E model. For tugs, both models showed significant variations (>15 dB) from the measured SLs, with the residual difference in R-B being smaller. For the tanker, research vessel, and container ships, the two models were in reasonable agreement (<5 dB) in terms of predicting SL. SLs of both models for the icebreaker, fishing vessel, and passenger ship were, however, significantly different (>17 dB). The residual difference between measurement and model predictions was further evaluated for all vessel types. Figures 11(a) and 11(b) display the residuals between the measured SL and the model calculations for R-B and J-E models, respectively. The R-B model has a mean absolute residual difference of less than 10 dB at low frequencies (0.5 kHz) but reaches a maximum of 15 dB above 0.5 kHz. The frequency averaged mean absolute residual difference between our measurements and the R-B model was 13 dB. Across the entire

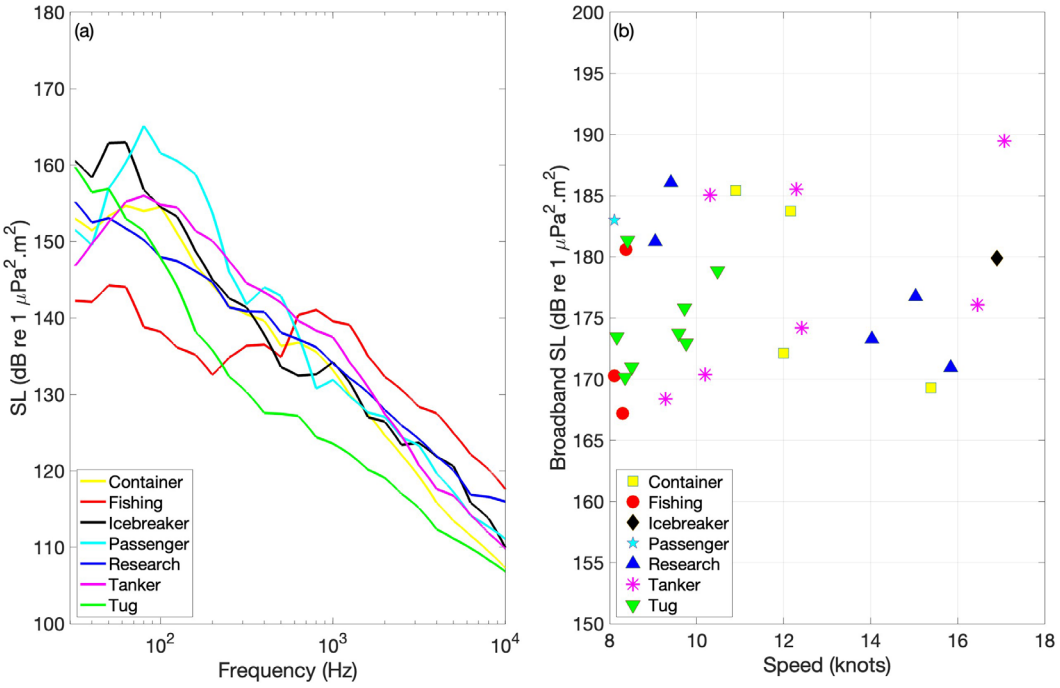

FIG. 8. (Color online) (a) The mean SLs of cavitating vessels for difference vessel types. (b) The broadband SLs of cavitating vessels as a function of speed.

https://doi.org/10.1121/10.0026361

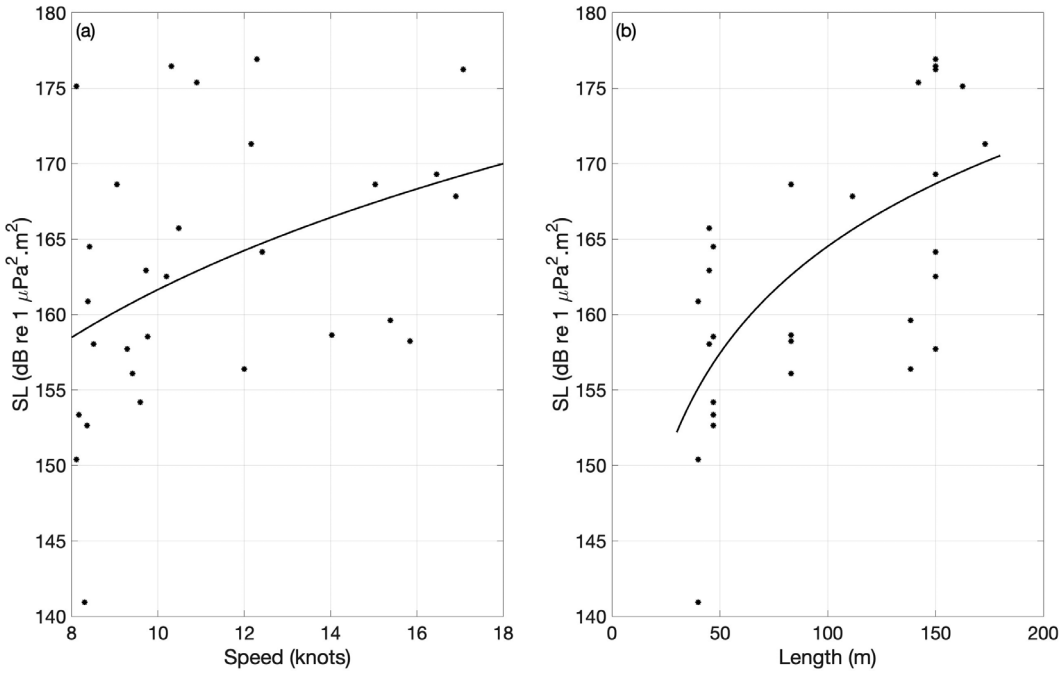

FIG. 9. Scatter plots of measure SLs vs (a) speed and (b) length in the 125 Hz decidecade band. Black solid curve is the fitted line.

frequency range, the J-E model showed better agreement with the measurements and the frequency averaged mean absolute residual difference was 8 dB.

Several factors might have contributed to the difference between model calculations and our measurements, including ship types, propagation conditions, independent PL models, and inter-study variability in data collection. The statistical uncertainty of J-E model was 6 dB, and the higher deviation between our measurements and model output suggests that the type of ships traveling in the Arctic may not be well represented in the model (MacGillivray and de Jong., 2021). Frequency averaged residual differences for tanker (3.5 dB), passenger vessel (1.3 dB), and container ships (3 dB) were within the model's statistical uncertainty. Research and fishing vessels had residual differences of 7.4 and 7.3 dB, respectively. Observed residual differences between measurements and model were highest for tugs (23 dB) and icebreaker (22 dB). In the validation dataset of the J-E model, these types of vessels are not well represented (MacGillivray and de Jong, 2021). Generally, ships traveling in the Arctic are classified as polar class vessels. A vessel of this class is generally designed with an ice-strengthened hull, stern, and propellers, enabling it to navigate the Arctic Ocean in ice-covered waters. Due to this, the

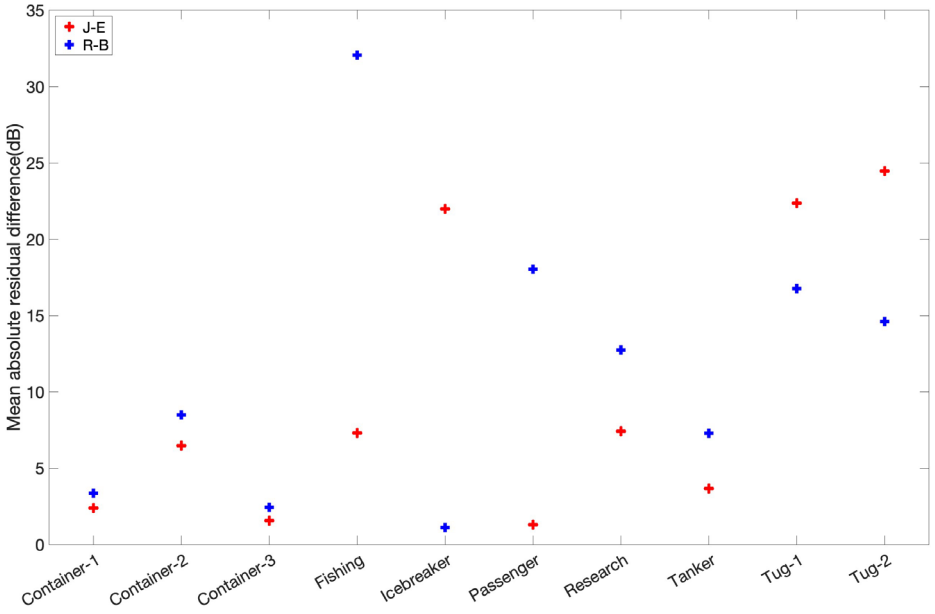

FIG. 10. (Color online) The mean absolute residual difference between measured SLs for individual vessels from the empirical models J-E and R-B.

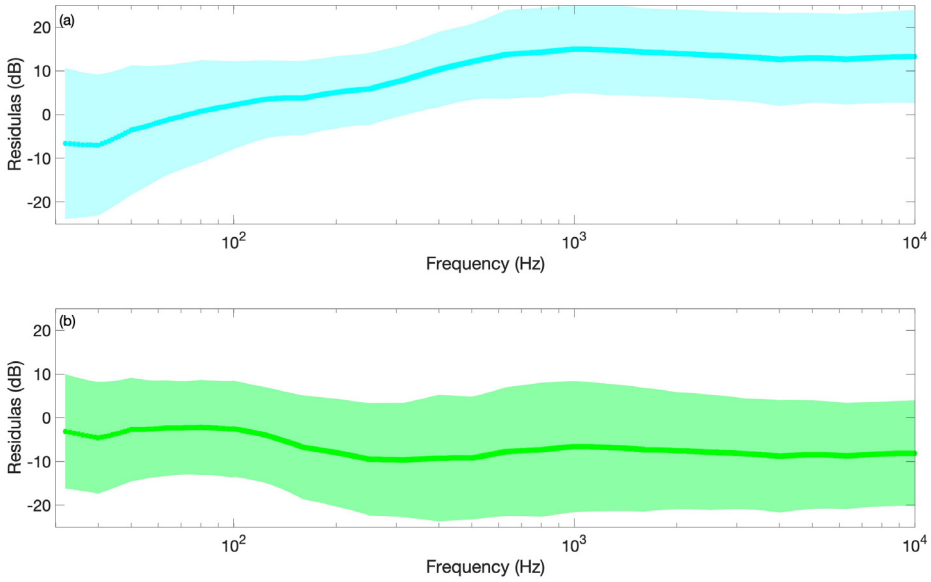

FIG. 11. (Color online) The mean residuals (line) and standard deviation (shaded area) between measured and modeled SLs for (a) RANDI-Breeding and (b) J-E.

sound generation and radiation characteristics of these vessels may differ from vessels traveling in other regions. Eighty-four percent of vessels traveling through the Northwest Passage between 2015 and 2019 were classified as polar class vessels, of which 55% were medium ice-strengthened to highly strengthened ships, while 29% were low ice-strengthened vessels (Dawson *et al.*, 2022). The vessels reported in this study are all polar class vessels with varying degrees of ice strengthening, and their characteristics are listed in Table III. As shown by the residual analysis, even though the J-E model is the best at representing Arctic ship SL data, more SL measurements are required for a thorough statistical analysis.

Finally, the SLs of cavitating vessels were also calculated using the seabed critical angle (SCA) method. The SCA method is a simplified equation for PL calculation derived as part of the latest effort to develop a standard for URN measurements in shallow water. The formula incorporates bottom loss through a term derived from SCA. Compared to a numerical sound propagation model, the SCA method produced robust SL estimates for URN measurements in shallow water (MacGillivray *et al.*, 2022, 2023). The mean residual difference between modeled SLs using the J-E model and measured SLs based on the SCA method is shown in Fig. 12(a). In comparison with the measured SLs calculated using the hybrid numerical model, the frequency averaged residual difference between the J-E model SLs and the measured SLs calculated with the SCA method was 6 dB or higher [Fig. 12(b)]. Since the SCA method works well at short ranges (<0.5 km), it underestimates PL at longer distances. Most of the CPA distances for cavitating vessels in this study were greater than 1 km (75%), which might have caused the large residual differences between SLs calculated with the SCA method and the J-E model.

TABLE III. Characteristics of vessels reported in this study.

Vessel type	Length	Polar class
Container 1	142	PC7
Container 2	173	PC7
Container 3	138.5	PC5
Passenger	162.6	PC5
Fishing	39	1A
Tug 1	46.7	1B
Tug 2	45.1	1B
Tug 3	52.4	1B
Tanker	150	PC5
Research (Icebreaker)	83	PC4
Icebreaker	111.5	PC4

3. Limitations

Here, we discuss the limitations associated with the measurement procedure and modeling used in this study. ANSI/ISO recommends multiple hydrophone measurements at different inclination angles (15°, 30°, and 45°) to improve SL measurement robustness and remove image interference. Single hydrophone opportunistic measurements in the Arctic pose a challenge to comply with ANSI/ISO inclination angles. SL calculations were made using an inclination angle as low as 4° in this study to incorporate more measurements. Without surface correction in PL calculation, low values of inclination angle can introduce uncertainty in SL estimates of 5–10 dB (Gassmann *et al.*, 2017). Because this study uses a numerical PL model that accounts for surface and bottom loss, the uncertainty due to low inclination angle can be reduced. In PAM systems with duty cycles, some measurements did not meet the ANSI/ISO DWP standards. For larger CPAs, the entire recording period was used to calculate RL metrics when DWP standards were not met. Clock drift associated with hydrophone recordings can also cause error in CPA and uncertainty in measured SLs (10% range error is equal to 0.5 dB in SL)

https://doi.org/10.1121/10.0026361

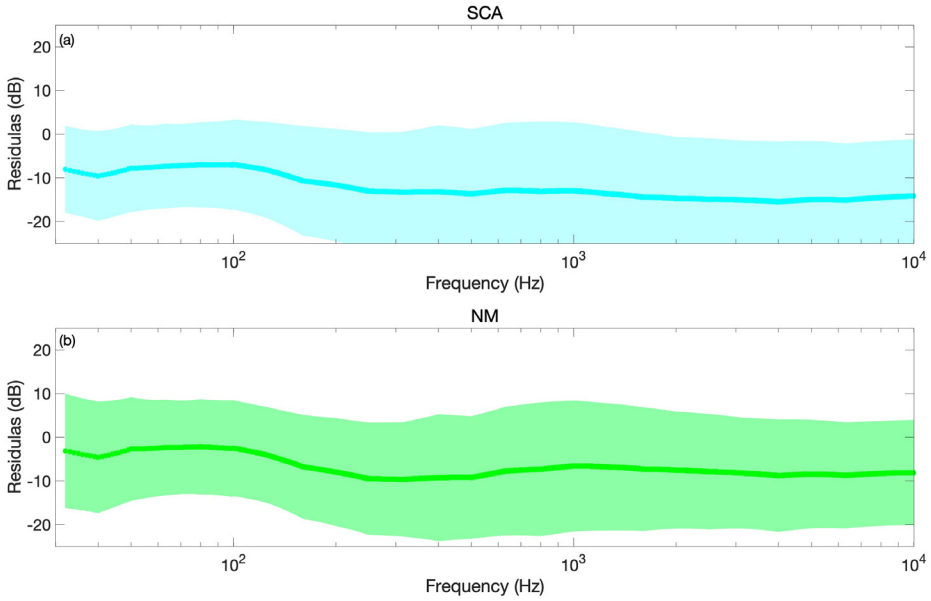

FIG. 12. (Color online) The mean residuals (line) and standard deviation (shaded area) between modeled SLs from the J-E model and measured SLs for (a) SCA method and (b) numerical model (NM). Only cavitating vessels are included in this comparison.

(MacGillivray *et al.*, 2022). AIS distance-time curves were aligned with acoustic data to determine clock drift, and time stamps were corrected using linear interpolation. In this study, PL was calculated by considering the ship source depth to be a point source at 6 m. At low frequencies, source depth variations of a few meters can introduce uncertainty of up to 4 dB [Fig. 4(c)]. The uncertainty associated with source depth can be minimized by using either a Gaussian distribution of source depths for PL calculation or adjusted SL (Wales and Heitmeyer, 2002; Ainslie *et al.*, 2022). Another drawback is the limited number of SL measurements for cavitating and non-cavitating vessels, which does not allow for a conclusive statistical analysis. We attempted to address the measurement and modeling limitations in this study, but these factors could still affect the measured SLs. It is difficult to precisely quantify the impact of these limitations on SL data uncertainty. However, the uncertainty associated with measured SLs will not significantly affect findings of this analysis considering the large mean residual difference between measured SLs and the J-E model for certain polar vessels.

IV. CONCLUSION

We presented a methodology for calculating the SL of vessels opportunistically using long-term passive acoustic data. The analysis was based on underwater acoustic data collected for soundscape monitoring in the Western Canadian Arctic. AIS information and acoustic data were combined to extract RL metrics from ship recordings. To account for the PL between the AIS vessel position and measurement location, we used a hybrid PL model. We calculated SLs at decidecade central frequencies and broadband SLs using a bandwidth from 31.5 Hz to 10 kHz. Based on cavitation inception speed, measured SLs were divided into cavitating and non-cavitating vessels. SL of non-cavitating vessels did not correlate well with vessel speed. Cavitating vessels, however, showed a positive correlation between SL and vessel speed. The SL to length slope of our measurements for cavitating vessels was comparable to the existing model results. Comparing measured SLs with existing SL models, J-E showed better agreement than R-B. The frequency averaged residual difference of research and fishing vessel, tugs, and an icebreaker were higher than the statistical uncertainty of the J-E model. Accordingly, the J-E model does not adequately represent certain polar class vessels operating in Arctic waters. Moreover, more than half of the measured SLs in this study are for non-cavitating vessels, which requires further investigation of the noise generation mechanism of polar class vessels at this speed range ($<$8 knots).

Passive acoustic data have been widely used for ocean observations, marine mammal monitoring, and soundscape studies. Ship noise monitoring using multiple hydrophones following ANSI standards is practically challenging in extreme environments, such as the Arctic. The results of this study show the advantage of soundscape monitoring data for opportunistic ship SL measurements in the Arctic. Climate change and an increase in economic, touristic, and marine scientific activity in the Arctic lead to an increase in ships traversing the Arctic during ice-free seasons every year. Thus, it is crucial to study the effects of increased shipping on the Arctic ecosystem. The functional relationship between the measured SL and the draft, breadth, and class of fleets traveling through the Arctic must also be investigated. A comprehensive study will require continuous monitoring of ship noise using multiple hydrophones in compliance with ANSI/ISO standards, along with better environmental information and more opportunistic SL measurements.

ACKNOWLEDGMENTS

All acoustic data used in this study were collected by Wildlife Conservation Society Canada, Fisheries and

Oceans Canada, and the Ekaluktutiak Hunters and Trappers Organization. We are grateful to collaborators in the communities of Cambridge Bay, Sachs Harbour, and Ulukhaktok who made the collection of data possible, including Wayne Gully and Adam Kudlak. We are also grateful to scientists and crew aboard the CCGS Sir Wilfrid Laurier, HMCS Saskatoon, and the R/V Martin Bergmann for assistance with deploying and recovering oceanographic moorings. Satellite AIS data from Spire Global (formerly exactEarth) were provided by the MEOPAR (Marine Environmental Observation, Prediction and Response) Network and the Meridian (Marine Environmental Research Infrastructure for Data Integration and Application Network) project. This work was supported by the Fisheries Joint Management Committee, Inuvialuit Game Council, the Hunters and Trappers Committees of Paulatuk, Sachs Harbour, and Ulukhaktok, the Ekaluktutiak Hunters and Trappers Organization, and Arctic Research Foundation. Funding for this work was provided by Fisheries and Oceans Canada (Oceans Management Contribution Program and Canada Nature Fund for Aquatic Species at Risk), Transport Canada, the Fisheries Joint Management Committee, World Wildlife Fund, and the W. Garfield Weston Foundation.

AUTHOR DECLARATIONS

Conflict of Interest

The authors declare that the research was conducted in the absence of any commercial or financial relationships that could be construed as a potential conflict of interest.

DATA AVAILABILITY

Data will be made available on request.

Ainslie, M. A., Martin, S. B., Trounce, K. B., Hannay, D. E., Eickmeier, J. M., Deveau, T. J., Lucke, K., MacGillivray, A. O., Nolet, V., and Borys, P. (**2022**). "International harmonization of procedures for measuring and analyzing of vessel underwater radiated noise," Mar. Pollut. Bull. **174**, 113124.

ANSI S12. *American National Standard: Quantities and Procedures for Description and Measurement of Underwater Sound from Ships. 1: General Requirements* (Acoustical Society of America, New York, **2009**).

Arveson, P. T., and Vendittis, D. J. (**2000**). "Radiated noise characteristics of a modern cargo ship," J. Acoust. Soc. Am. **107**, 118–129.

Aulanier, F., Simard, Y., Roy, N., Gervaise, C., and Bandet, M. (**2017**). "Effects of shipping on marine acoustic habitats in Canadian Arctic estimated via probabilistic modeling and mapping," Mar. Pollut. Bull. **125**, 115–131.

Breeding, J. E., Jr., Pflug, L. A., Bradley, M., Walrod, M. H., and McBride, W. (**1996**). "Research ambient noise directionality (RANDI) 3.1 physics description," *NRL Report Naval Research Laboratory* (Stennis Space Center, Hancock County, MS).

Chapman, N. R., and Price, A. (**2011**). "Low frequency deep ocean ambient noise trend in the Northeast Pacific Ocean," J. Acoust. Soc. Am. **129**, 161–165.

Chen, C., Lin, T. H., Watanabe, H. K., Akamatsu, T., and Kawagucci, S. (**2021**). "Baseline soundscapes of deep sea habitats reveal heterogeneity among ecosystems and sensitivity to anthropogenic impacts," Limnol. Oceanogr. **66**, 3714–3727.

Chion, C., Lagrois, D., and Dupras, J. (**2019**). "A meta analysis to understand the variability in reported source levels of noise radiated by ships from opportunistic studies," Front. Mar. Sci. **6**, 714.

Dawson, J., Cook, A., Holloway, J., and Copland, L. (**2022**). "Analysis of changing levels of ice strengthening (Ice Class) among vessels operating in the Canadian Arctic over the past 30 years," Arctic **75**, 413–430.

Deane, G. B. (**1997**). "Sound generation and air entrainment by breaking waves in the surf zone," J. Acoust. Soc. Am. **102**, 2671–2689.

Duarte, C. M., Chapius, L., Collin, S. P., Costa, D. P., Devassy, R. P., Eguiluz, V. M., Erbe, C., Gordon, T. A. C., Halpern, B. S., Harding, H. R., Havlik, M. N., Meekan, M., Merchant, N. D., Miksis-Olds, J. L., Parsons, M., Predragovic, M., Radford, A. N., Radford, C. A., Simpson, S. D., Slabbekoorn, H., Staaterman, E., Van Opzeeland, I. C., Winderen, J., Zhang, X., and Juanes, F. (**2021**). "The soundscape of the Anthropocene ocean," Science **371**, eaba4658.

Eguilus, V. M., Fernandez-Gracia, J., Irigoien, X., and Duarte, C. M. (**2016**). "OPEN a quantitative assessment of Arctic shipping," Sci. Rep. **6**, 30682.

Erbe, C., MacGillivray, A., and Williams, R. (**2012**). "Mapping cumulative noise from shipping to inform marine spatial planning," J. Acoust. Soc. Am. **132**, EL423–EL428.

Erbe, C., Schoeman, R. P., Peel, D., and Smith, J. N. (**2021**). "It often howls more than it chugs: Wind versus ship noise underwater in Australia's maritime regions," J. Mar. Sci. Eng. **9**, 472.

Farcas, A., Powell, C. F., Brookes, K. L., and Merchant, N. D. (**2020**). "Validated shipping noise maps of the Northeast Atlantic," Sci. Total Environ. **735**, 139509.

Frisk, G. V. (**2012**). "Noiseonomics: The relationship between ambient noise levels in the sea and global economic trends," Sci. Rep. **2**, 437.

Gassmann, M., Wiggins, S. M., and Hildebrand, J. A. (**2017**). "Deep-water measurements of container ship radiated noise signatures and directionality," J. Acoust. Soc. Am. **142**, 1563–1574.

Halliday, W. D., Barclay, D., Barkley, A. N., Cook, E., Dawson, J., Hilliard, R. C., Hussey, N., Jones, J., Juanes, F., Marcoux, M., Niemi, A., Nudds, S., Pine, M. K., Richards, C., Scharffenberg, K., Westdal, K., and Insley, S. J. (**2021**). "Underwater sound levels in the Canadian Arctic, 2014–2019," Mar. Pollut. Bull. **168**, 112437.

Halliday, W. D., Dawson, J., Yurkowski, D. J., Doniol-Valcore, T., Ferguson, S. H., Gjerdrum, C., Hussey, N. E., Kochanowicz, Z., Mallory, M. L., Marcoux, M., Watt, C. W., and Wong, S. N. P. (**2022**). "Vessel risks to marine wildlife in the Tallurutiup Imanga National Marine Conservation Area and the eastern entrance to the Northwest Passage," Environ. Sci. Pollut. **127**, 181–195.

Halliday, W. D., Insley, S. J., Hiliard, R. C., Jong, T. D., and Pine, M. K. (**2017**). "Potential impacts of shipping noise on marine mammals in the western Canadian Arctic," Mar. Pollut. Bull. **123**, 73–82.

Halliday, W. D., Pine, M. K., Citta, J., Harwood, L., Hauser, D. D. W., Hilliard, R. C., Lea, E., Loseto, L. L., Quakenbush, L., and Insley, S. J. (**2021**). "Potential exposure of beluga and bowhead whales to underwater noise from ship traffic in the Beaufort and Chukchi Seas," Ocean Coast Manage. **204**, 105473.

Halliday, W. D., Pine, M. K., Mouy, X., Kortsalo, P., Hilliard, R. C., and Insley, S. J. (**2020**). "The coastal Arctic marine soundscape near Ulukhaktok," Pollut. Biol. **43**, 623–636.

Hamilton, E. L. (**1980**). "Geoacoustic modeling of the sea floor," J. Acoust. Soc. Am. **68**, 1313–1340.

Harris, P., Sotirakopoulos, K., Robinson, S., Wang, L., and Livina, V. (**2019**). "A statistical method for the evaluation of long term trends in underwater noise measurements," J. Acoust. Soc. Am. **145**, 228–242.

Harrison, C. H., and Harrison, J. A. (**1995**). "A simple relationship between frequency and range averages for broadband sonar," J. Acoust. Soc. Am. **97**, 1314–1317.

Hersbach, H., Bell, B., Berrisford, P., Hirahara, S., Horanyi, A., Munoz-Sabater, J., Nicolas, J., Peubey, C., Radu, R., Schepers, D., Simmons, A., Soci, C., Abdalla, S., Abellan, X., Balsamo, G., Bechtold, P., Biavati, G., Bidlot, J., Bonavita, M., De-Chiara, G., Dahlgren, P., Dee, D., Diamantakis, M., Dragani, R., Flemming, J., Forbes, R., Fuentes, M., Geer, A., Haimberger, L., Healy, S., Hogan, R. J., Hoolm, E., Janiskova, M., Keeley, S., Laloyaux, P., Lopez, P., Lupu, C., Radnoti, G., de Rosnay, P., Rozum, I., Vamborg, F., Villaume, S., and Thepaut, J.-N. (**2020**). "The ERA5 global reanalysis," Q. J. R. Meteorol. Soc. **146**, 1999–2049.

Hildebrand, J. A., Frasier, K. E., Pickering, S. B., and Wiggins, S. M. (**2021**). "An empirical model for wind-generated noise," J. Acoust. Soc. Am. **149**, 4516–4533.
Howe, B. M., Miksis-Olds, J. L., Rehm, E., Sagen, H., Worcester, P. F., and Haralabus, G. (**2019**). "Observing the oceans acoustically," Front. Mar. Sci. **6**, 426.
Insley, S. J., Halliday, W. D., and de Jong, T. (**2017**). "Seasonal patterns in ocean ambient noise near Sachs Harbour, Northwest Territories," Arctic **70**, 239–248.
ISO 17208-1:2016 (**2016**). "Underwater acoustics: Quantities and procedures for description and measurement of underwater sound from ships. Part 1: Requirements for precision measurements in deep water used for comparison purposes" (International Organization for Standardization, Geneva, Switzerland).
ISO 18405:2017 (**2017**). "Underwater acoustics: Terminology" (International Organization for Standardization, Geneva, Switzerland).
ISO 17208-2:2019 (**2019**). "Underwater acoustics: Quantities and procedures for description and measurement of underwater sound from ships. Part 2: Determination of source levels from deep water measurements" (International Organization for Standardization, Geneva, Switzerland).
Jansen, E., and de Jong, C. (**2017**). "Experimental assessment of underwater acoustic source levels of different ship types," IEEE J. Ocean Eng. **42**, 439–448.
Jensen, F. B., Kuperman, W. A., Porter, M. B., and Schmidt, H. (**2011**). *Computational Ocean Acoustics* (Springer, New York).
Karasalo, I., Ostberg, M., Sigray, P., Jalkanen, J. P., Johansson, L., Liefvendahl, M., and Bensow, R. (**2017**). "Estimates of source spectra of ships from long term recordings in the Baltic," Front. Mar. Sci. **4**, 164.
Lataief, S., Montero-Serrano, J.-C., and St-Onge, G. (**2021**). "Sedimentary processes within the Canadian Arctic Archipelago: Relationships among sedimentological, geochemical and magnetic sediment properties," Geochem. Geophys. Geosyst. **22**, e2021GC009719.
Leaper, R., Renilson, M., and Ryan, C. (**2014**). "Reducing underwater noise from large commercial ships: Current status and future directions," J. Ocean Tech. **9**(1), 51–69.
Li, X., Stephenson, S. R., Lynch, A. H., Goldstein, M. A., Bailey, D. A., and Veland, S. (**2021**). "Arctic shipping guidance from the CMIP6 ensemble on operational and infrastructural timescales," Climate Change **167**, 23.
Lin, Y. T., Duda, T. F., and Newhall, A. E. (**2013**). "Three-dimensional sound propagation models using the parabolic-equation approximation and the split-step Fourier method," J. Comput. Acoust. **21**, 1250018.
Ma, B. B., Nystuen, J. A., and Lien, R. C. (**2005**). "Prediction of underwater sound levels from rain and wind," J. Acoust. Soc. Am. **117**, 3555–3565.
MacGillivray, A. O., Ainsworth, L. M., Zhao, J., Dolman, J. N., Hannay, D. E., Frouin-Mouy, H., Trounce, K. B., and White, D. E. (**2022**). "A functional regression analysis of vessel source level measurements from the Enhancing Cetacean Habitat and Observation (ECHO) database," J. Acoust. Soc. Am. **152**, 1547–1563.
MacGillivray, A. O., and de Jong, C. A. F. (**2021**). "A reference spectrum model for estimating source levels of marine shipping based on Automated Identification System data," J. Mar. Sci. Eng. **9**, 369.
MacGillivray, A. O., Li, Z., Hannay, D. E., Trounce, K. B., and Robinson, O. M. (**2019**). "Slowing deep sea commercial vessels reduces underwater radiated noise," J. Acoust. Soc. Am. **146**, 340–351.
MacGillivray, A. O., Martin, S. B., Ainslie, M. A., Dolman, J. N., Li, Z., and Warner, G. A. (**2023**). "Measuring vessel underwater radiated noise in shallow water," J. Acoust. Soc. Am. **153**, 1506–1524.
MacGillivray, A. O., Martin, S. B., Ainslie, M. A., Dolman, J. N., Li, Z., Warner, G. A., Lawrence, C. B., Pace, F., Schuster, M., and Wittekind, D. (**2022**). "Towards a standard for vessel URN measurement in shallow water," Technical Report, Document No. 02427, version 2.0, JASCO Applied Sciences, Nova Scotia, Canada.
McDonald, M. A., Hildebrand, J. A., and Wiggins, S. M. (**2006**). "Increases in deep ocean ambient noise in the Northeast Pacific west of San Nicolas Island, California," J. Acoust. Soc. Am. **120**, 711–718.
McKenna, M. F., Ross, D., Wiggins, S. M., and Hildebrand, J. A. (**2012**). "Underwater radiated noise from modern commercial ships," J. Acoust. Soc. Am. **131**, 92–103.
McKenna, M. F., Wiggins, S. M., and Hildebrand, J. A. (**2013**). "Relationship between container ship underwater noise levels and ship design, operational and oceanographic conditions," Sci. Rep. **3**, 1760.
Merchant, N. D., Pirotta, E., Barton, T. R., and Thompson, P. M. (**2014**). "Monitoring ship noise to assess the impact of coastal developments on marine mammals," Mar. Pollut. Bull. **78**, 85–95.
Meredith, M., Sommerkorn, M., Cassotta, S., Derksen, C., Ekaykin, A., Hollowed, A., Kofinas, G., Mackintosh, A., Melbourne-Thomas, J., Muelbert, M. M. C., Ottersen, G., Prichard, H., and Schuur, E. A. G. (**2019**). "Polar regions," in *IPCC Special Report on the Ocean and Cryosphere in Changing Climate*, edited by H.-O. Portner, D. C. Roberts, V. Masson-Delmotte, P. Zhai, M. Tignor, E. Poloczanska, K. Mintenbeck, A. Algria, M. Nicolai, A. Okem, J. Petzold, B. Rama, and N. M. Weyer (Cambridge University Press, Cambridge, UK), pp. 203-320.
Miksis-Olds, J. L., Martin, B., and Tyack, P. L. (**2018**). "Exploring the ocean through soundscapes," Acoust. Today **14**, 26–34.
Miksis-Olds, J. L., and Nichols, S. M. (**2016**). "Is low frequency ocean sound increasing globally?" J. Acoust. Soc. Am. **139**, 501–511.
Pine, M. K., Hannay, D. E., Insley, S. J., Halliday, W. D., and Juanes, F. (**2018**). "Assessing vessel slowdown for reducing auditory masking for marine mammals and fish of the western Canadian Arctic," Mar. Pollut. Bull. **135**, 290–302.
Pizzolato, L., Howell, S., Dawson, J., Laliberte, F., and Copland, L. (**2016**). "The influence of declining sea ice on shipping activity in the Canadian Arctic," Geophys. Res. Lett. **43**, 12146–12154, https://doi.org/10.1002/2016GL071489.
Porter, M. B. (**2016**). "Bellhop3d user guide," *Techical Report* (Heat, Light, & Sound Research Inc., La Jolla, CA).
Porter, M. B., and Bucker, H. P. (**1987**). "Gaussian beam tracing for computing ocean acoustic," J. Acoust. Soc. Am. **82**, 1349–1359.
Putland, R. L., de Jong, C. A. F., Binnerts, B., Farcas, A., and Merchant, N. D. (**2022**). "Multi-site validation of shipping noise maps using field measurements," Mar. Pollut. Bull. **179**, 113733.
Ross, D. (**1976**). *Mechanics of Underwater Noise* (Pergamon Press, New York).
Ross, D. (**2005**). "Ship sources of ambient noise," IEEE J. Ocean Eng. **30**, 257–261.
Ross, D., and Alvarez, F. F. (**1964**). "Radiated underwater noise of surface ships," US Navy. J. Underw. Acoust. **14**, 331.
Ryan, W., Carbotte, S., Coplan, J., O'Hara, S., Melkonian, A., Arko, R., Weissel, R., Ferrini, V., Goodwillie, A., Nitsche, F., Bonczkowski, J., and Zemsky, R. (**2009**). "Global Multi-Resolution Topography (GMRT) synthesis data set," Geochem. Geophys. Geosyst. **10**(3), Q03014.
Simard, Y., Roy, N., Gervaise, C., and Giard, S. (**2016**). "Analysis and modeling of 255 source levels of merchant ships from an acoustic observatory along St. Lawrence," J. Acoust. Soc. Am. **140**, 2002–2018.
Smith, J. A., and Rigby, J. (**2022**). "Underwater radiated noise from marine vessels: A review of noise reduction methods and technology," Ocean Eng. **266**, 112863.
Stephenson, S. R., Smith, L. C., and Agnew, J. A. (**2011**). "Divergent long-term trajectories of human access to the Arctic," Nat. Climate Change **1**, 156–160.
Tappert, F. D. (**1974**). "Parabolic equation method in underwater acoustics," J. Acoust. Soc. Am. **55**, S34.
Urick, R. J. (**1983**). *Principles of Underwater Sound* (McGraw-Hill, New York).
Vagle, S., Large, W. G., and Farmer, D. M. (**1990**). "An evaluation of the WOTAN technique of inferring oceanic winds from underwater ambient sound," J. Atmos. Ocean Tech. **7**, 576–595.
Vendittis, D. J., and Arveson, P. T. (**2022**). "Ten challenges in measuring and reporting ship noise levels," JASA Express Lett. **2**, 036801.
Wales, S. C., and Heitmeyer, R. M. (**2002**). "An ensemble source spectra model for merchant ship radiated noise," J. Acoust. Soc. Am. **111**, 1211–1231.
Wittekind, K. A. (**2014**). "A simple model for the underwater noise source level of ships," J. Ship Production Design **30**, 1–8.
Wenz, G. M. (**1962**). "Acoustic ambient noise in the ocean: Spectra and sources," J. Acoust. Soc. Am. **34**, 1936–1956.